Volume 10, Issue 3, 2020, 5640 - 5647 ISSN 2069-5837

Biointerface Research in Applied Chemistry

www.BiointerfaceResearch.com

https://doi.org/10.33263/BRIAC103.640647

Original Research Article Open Access Journal

Received: 14.02.2020 / Revised: 20.03.2020 / Accepted: 21.03.2020 / Published on-line: 29.03.2020

Preparation of natural rubber-OMMT nanocomposites using mechanical mixing and acid free co-coagulation methods: effect of processing method on mechanical properties

Sudarshana Jayaraj Perara [1], Shantha Egodage[1,*], Shantha Walpalage [1]

[1]Department of Chemical and Process Engineering, University of Moratuwa, Sri Lanka

*corresponding author e-mail address: ***segodage@uom.lk; sudarshana79@gmail.com*** | Scopus ID 28067786200

ABSTRACT

The masterbatches were prepared by acid free co-coagulation (AFCC) method in which OMMT was incorporated into natural rubber latex (NRL) or conventional mechanical mixing. Inherent slow coagulation, and drying, stages of the AFCC method were overcome by introducing a novel gelling agent; a combination of two surfactants, namely, Cetyl tri methyl ammonium bromide (CTAB) and Sodium dodecyl sulphate (SDS). Six nanocomposites (A-nanocomposite, C-nanocomposite and M-nanocomposite) were prepared at the OMMT loadings of 2 and 5 phr; of them, two with gelling agent (A-2, A-5) and two without gelling agent (C-2, C-5) using AFCC method and two using mechanical mixing (M-2 & M-5). Controls of them (A-0, C-0 and M-0) were prepared without using OMMT. X-ray diffractograms and scanning electron spectroscopic images showed that a higher amount of aggregated clay structures was present in the M-nanocomposites, and less aggregated clay structures were present in C-nanocomposites. However randomly distributed ordered structures along with exfoliated clay structures were in the A-nanocomposites. Crosslink density and the bound rubber content of the A-nanocomposites were significantly higher than M-nanocomposites but lower than C-nanocomposites. The mechanical properties of the A- nanocomposites and C-nanocomposites were greater than those of the M-nanocomposites at each OMMT loading. The cure time of the A-nanocomposites and C-nanocomposites were also remarkably lowered compared to the M-nanocomposites. It was observed that the effect of the combined gelling agent had no adverse effect on mechanical properties.

Keywords: *Nanocomposite; Co-coagulation; Gelling agent; Mechanical properties; Natural rubber; Organo clay; Rubber compounding.*

1. INTRODUCTION

Natural rubber (NR) based products are highly demanded due to remarkable properties of NR not shared in other materials. The greater mechanical properties of NR are the main reason for its use in manufacturing many rubber products. It is also well known that mechanical properties of NR could be further increased by addition of fillers [1-3] and use of them with different processing techniques [4-6]. These properties include tensile strength, elongation at break, tear strength, modulus at 300% and hardness. Carbon black, silica, calcium carbonate, kaolin and mica are used as conventional fillers in enhancing such properties. It was noted that high loading is necessary to increase the properties, but is difficult to improve all at once. In recent years, nano-fillers like nanoclays have attracted attention due to their ability to enhance the mechanical properties of nanocomposites at low clay loadings [7,8].

Montmorillonite (MMT) is widely used to prepare nanocomposites due to its availability, intercalation/exfoliation chemistry, high surface area and excellent swelling behavior over the other types of clays like kaolin [9]. However, the mechanical properties were not improved when MMT was incorporated into NR due to lack of rubber-filler interactions created between non-polar NR and polar MMT [10]. MMT was not properly dispersed in NR produced by mechanical mixing, the most widely practiced method in the industry incorporating fillers into rubbers. Replacement of MMT by organically modified MMT (OMMT) was suggested as the best option to develop rubber-filler interactions and to achieve enhanced mechanical properties [11]. However, the property enhancement was limited due to the formation of aggregated clay structures [12]. The prevention of aggregation of clay layers and retention of nanostructures like intercalated and exfoliated clay structures in the nanocomposites are the major challenges. Therefore, it is necessary to develop an efficient method for the incorporation of OMMT into NR.

In one of our previous studies [13], MMT filled NR nanocomposite masterbatches were produced by acid free co-coagulation (AFCC) method starting from the latex stage and the dried sheets were compounded with other ingredient using conventional mechanical mixing, and obtained good mechanical properties. Emulsion blending is also developed in rubber filler mixing as an efficient method to incorporate fillers into rubber latex [14]. It was successfully used with AFCC method in previous studies [13,14].

However, OMMT is rarely incorporated at the latex stage due to the difficulty in handling OMMT as an aqueous suspension. In another study [15], Cetyl trimethyl ammonium bromide (CTAB) modified MMT was used in NR nanocomposite masterbatches and obtained better mechanical properties at lower OMMT loadings. It is also identified that commercial organoclay surface was modified with quaternary ammonium cation to obtain better dispersion in a novel study [16] However, it was identified that slow coagulation and drying steps in the AFCC method are the main drawbacks to produce nanocomposite in an industrial

scale. This study focuses on modifying the AFCC method by introducing a gelling agent, especially to overcome the drawbacks of clay aggregation and slow drying. The effect of gelling agent on the mechanical properties of the nanocomposites was also evaluated.

2. MATERIALS AND METHODS

High ammonia preserved centrifuged NRL, was purchased from Hanwalla Rubber (pvt) Ltd, Sri Lanka and pale crepe, a type of raw dry rubber was supplied by Samson Compounds PLC, Sri Lanka. Those were used in preparation of NR-clay nanocomposite masterbatches by AFCC method. Sodium montmorillonite clay (MMT) was used as a reinforcing filler and was supplied by Southern Clay Products, USA, under the trade name of Cloisite-116. MMT has a cation exchange capacity (CEC) of 80 meq/100 g and an interlayer distance of 1.25 nm (in non- hydrous form). Cetyl trimethyl ammonium bromide (CTAB) and Sodium dodecyl sulfate (SDS) in the combine gelling agent were purchased from GloChem (Pvt) Ltd, Sri Lanka. Sulfur (Rub-O-Sulf) as the vulcanizing agent, mercaptobenzothiazole sulphanamide (Murcure MBTS, Merchem) as the accelerator, zinc oxide (White seal; ACPL-P999) as the inorganic activator, stearic acid (Lubstric, Godrej industries Ltd) as the organic activator, and phenolic type Antioxidant (Lowinox CPL, Chempoint) were used in this study as per the formulation given in Table 1.

3 wt% aqueous suspension of MMT was prepared in mixing MMT with distilled water at 40-50 °C under vigorous stirring using a magnetic stirrer. Further stirring was carried out by means of an attrition mill (01HD made in Union Process, USA), operated at 600 rpm for 30 minutes and using ultrasonic stirrer (Qsonica, USA) operated at a frequency of 20 kHz frequency for 15 minutes. 18 millimoles of CTAB in water was then added into MMT suspension and mixed using the attrition mill and the ultrasonic stirrer under the same operating condition. The suspension was left aside overnight and the product was filtered. The de-watered suspension was washed several times with distilled water using vacuum filtration until no white precipitate was observed with 0.1 M $AgNO_3$. Finally, bromide free CTAB modified MMT was prepared as a de-watered suspension. It was dried in a vacuum oven at 60 °C for 2 days. The resultant OMMT crystals were then ground using a mortar and pestle into a fine powder.

A paste was prepared by mixing of OMMT powder with 15 wt% Dispersol LR together with a small quantity of distilled water. After that 3 wt% OMMT suspension was prepared by mixing of the paste with distilled water using a mechanical stirrer at a speed of 200 rpm followed by further mixing in the attrition mill and the ultrasonic stirrer under the previous processing conditions.

2 and 5 phr loadings of OMMT in the form of suspensions were added into de-ammoniated centrifuged NRL in presence of 1 phr loading of 10 wt% SDS dispersion and mixed using the mechanical stirrer at a speed of 60 rpm for 24 hours (emulsion blending). 2 phr loading of 10 wt% CTAB dispersion was mixed with, NRL-OMMT mix in the aluminum pans for gelling. The resultant gels were pressed by hand and were dried in the air circulated oven at 50 °C for one day. The dried sheets were milled to obtain sheets having even thickness and were dried again for another two days in a smoke house under similar condition used in preparation of ribbed smoke rubber sheet. The NR-OMMT masterbatches prepared were named as A-2 (2 phr of OMMT) and A-5 (5 phr of OMMT). The Control without addition of OMMT prepared in above method is considered as A-0. The masterbatches prepared without addition of gelling agent were called C-2 (2 phr OMMT), C-5 (5 phr OMMT) and the Control without OMMT was named as C-0. The masterbatches of M-2 and M-5 (2 and 5 phr, loadings OMMT) and M-0 (Control, without OMMT) were prepared by mechanical mixing with pale crepe rubber.

Zinc oxide, stearic acid and antioxidants were incorporated into all NR-clay masterbatches and controls as per the formulation given in Table 2, using the Brabender plasticorder operated at a speed of 60 rpm for 5 minutes. Sulphur and MBTS were then added to the compounds using a two-roll mill for another 2 minutes to prepare nanocomposite compounds.

The nanocomposite compounds were vulcanized to obtain final nanocomposite using a hydraulic press (model Moore made in England) at 140 °C under 15 MPa pressure for the respective cure times, $t_{90,}$ determined from the cure curves.

Cure characteristics of nanocomposite compounds were obtained from rubber process analyzer (RPA flex, USA) operated at a temperature of 140 °C as per ASTM standard D 2048-95. Maximum torque (M_H) and minimum torque (M_L), cure time that represents the time for a rise by two units from minimum torque (t_{s2}) and cure time that corresponds to 90% of cure (t_{90}) were determined. The cure rate index (CRI) is expressed as Equation (1).

$$CRI = \frac{100}{t_{90} - t_{s_2}} \qquad (1)$$

Nanocomposites were fractured under liquid nitrogen and their Scanning electron microscopy (SEM) images were taken using a scanning electron microscope of the model Evo 18 made in Carl-Zeiss, Germany. Fracture surfaces were gold sputter coated to prevent charging under the electron beam.

X-ray diffraction (XRD) technique was used to evaluate the structural behaviour of nanocomposites at a wavelength of 1.54 Å of Cu Kα radiation using a model D8 advance diffractometer made in Bruker, Germany. Scanning was carried out over a Bragg angle (2θ) ranging from 4 – 8° at a rate of 0.01° of step size. Interlayer-gallery space, d, of MMT was calculated using the conventional Bragg equation, given by equation (2).

$$n\lambda = 2d \sin\theta \qquad (2)$$

where, λ - Wave length of X-rays

θ- Angle between incident radiation and scattering plan

n - Order of diffraction

Specimen from nanocomposites having dimensions of 20 mm×20 mm×2 mm was immersed in toluene for 48 hours in dark environment and were dried in a vacuum oven at 60 °C until constant weight was achieved. Weights of a specimen before swelling, swollen gel, and after drying, were recorded and were used to determine crosslink density. Volume fraction, v, is defined as the crosslink density by mol per gram and is given by equation (3).

$$v = {}^{1}/_{2\,M_c} \qquad (3)$$

Where M_c is the molar mass between the crosslink of rubber vulcanizate and it was calculated by Flory-Rehner equation [17], which is given by equation (4)

$$M_c = \frac{-\rho_r \times V_s \times V_r^{1/3}}{\ln(1-V_r) + (V_r + \varkappa V_r^2)} \qquad (4)$$

Where, ρ_r - density of NR (0.92 gcm^{-3})

V_s - Molar volume of toluene (106.35 cm^3mol^{-1})

$\varkappa$ - Flory-Hugging polymer-solvent interaction, (0.39) for NR-toluene

V_r - volume of fraction of rubber in swollen gel

V_r was calculated using Ellis and Welding equation [18] as given in Equation (5).

$$V_r = \frac{(D-FW)\rho_r}{\frac{(D-FW)}{\rho_r} + \frac{A_o}{\rho_s}} \qquad (5)$$

Where, A_o - weight of absorbed solvent

ρ_s - Density of solvent (0.87)

D - De-swollen weight

F - Weight fraction of the filler

W - Initial weight of the sample

0.2 g of each masterbatch was cut into small pieces of approximately 1 mm^3 in size and was placed into a stainless steel cage of a known weight. The cage was then immersed in 50 ml of toluene at room temperature for 72 hours. Masterbatch specimens were taken out and vacuum dried at 60 °C to a constant weight. Bound rubber content was measured, according to equation (6) [19].

$$\text{Bound rubber content} = \frac{W_{fg} - W[m_f/(m_f+m_p)]}{W[m_p/(m_f+m_p)]} / \times 100 \qquad (6)$$

Where w_{fg} the weight of MMT is added, m_f is the weight of the filler in the masterbatch, m_p is the weight of the polymer in the masterbatch, and W is the weight of the specimen.

Dynamic mechanical thermal analysis (DMTA) of masterbatch was carried out using a Dynamic mechanical analyzer of model Q 800 of TA instrument, USA. The dual cantilever mode of deformation was selected. Rectangular test specimens having dimensions of 40 mm x 12 mm x 2 mm were examined over temperature a range of -80 °C to 80 °C, at a heating rate of 2 °C/min. Liquid nitrogen was used as the cooling medium. tan δ of each masterbatch was recorded in temperature sweep mode at 1.0 Hz.

Tensile properties such as tensile strength, elongation at break and modulus at 300% elongation (mod 300%), and tear strength were measured using Hounsfield H10KT tensile tester as per ISO 37:2011 and ISO 34-1:2010, respectively. Dumbbell specimens (type1) and angle specimens were punched from 2 mm thick vulcanized sheets and strained at a rate of 500 mm/min. Crosshead movement was taken as the extension. Hardness of nanocomposite was determined using a dead load hardness tester of model H14/PC made in Wallace Instruments, UK according to ISO 48:2010. Specimen having a thickness of 12.5 ± 0.5 mm and diameter of 29.0 ± 0.5 mm were used.

Abrasion loss of a nanocomposite was measured according to ASTM D5963-04(2015) using electromechanical abrasion tester of model Zwick 6102 made in USA. The cylindrical shape specimens having diameter of 16 ± 0.3 mm and height 6 mm, were kept on a rotating sample holder and 5 N load was applied. The abrasion loss was calculated according to equation (7)

$$\Delta V = \frac{\Delta m}{\rho} \qquad (7)$$

Where Δm the mass loss of sample is during the abrasion test, ρ is the density of the specimen and ΔV is the abrasion loss in cm^3.

Table 1. Formulation of NR-OMMT masterbatches and Controls.

	Loading, phr								
Ingredients	A-0	A-2	A-5	C-0	C-2	C-5	M-0	M-2	M-5
NR-clay MB	100	100	100	100	100	100	-	-	-
Crepe Rubber	-	-	-	-	-	-	100	100	100
OMMT	-	2	5	-	2	5	-	2	5
CTAB	2	2	2	-	-	-	-	-	-
SDS	1	1	1	-	-	-	-	-	-

Table 2. Formulation of Nanocomposite compound.

Ingredients	Loading, phr
NR-clay MB	100
Sulphur	2
ZnO	5
Stearic acid	2
MBTS	2
Antioxidant	1

3. RESULTS

3.1. Cure characteristics.

Figure 1 shows t_{s2} , t_{90} and CRI of nanocomposite compounds, A, C, M and their Controls A-0, C-0 and M-0 respectively.

A series compounds show lower t_{s2} and t_{90} values compared to M series compounds and C series compounds and are due to a higher number of CTAB and thereby increasing the amount of zinc-ammine complexes in nanocomposite compounds. It is believed that tertiary amine formed by Hoffman degradation of quaternary amine may form zinc ammine complexes [20]. The masterbatches prepared using AFCC rubber contains more non-rubber substances and hence C-series compounds compared to

M-series compounds showed lower t_{s2} and t_{90} of their control samples.

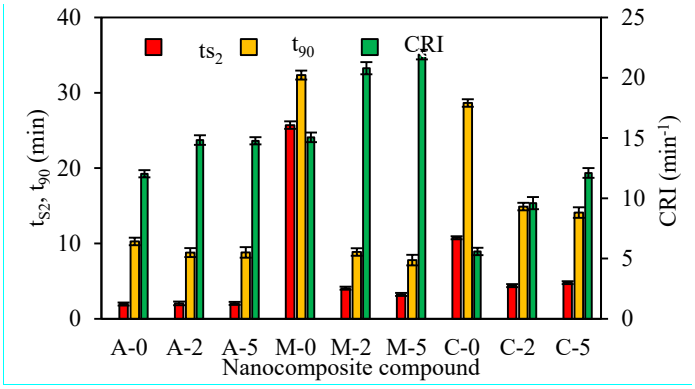

Figure 1. t_{s2},t_{90} and CRI of A, M & C nanocomposite compounds.

A higher amount of non-rubber substances remained in masterbatches prepared using AFCC method because only water was evaporated [13,14]. t_{s2} and t_{90} of C and M nanocomposite compounds show lower values than their controls due to addition of CTAB via OMMT. However, due to the formation of confined clay structures with CTAB, the release of degraded amine from CTAB in the formation of zinc-ammine complexes may be slow and hence t_{s2} and t_{90} of C-series nanocomposite compounds increased than that of M-series nanocomposites compounds. The CTAB is added only via OMMT in both C-nanocomposite and M-nanocomposite, in which CTAB is found as confined in the inter gallery space of clay. Better dispersion of limited OMMT in C-nanocomposite compounds may decrease Hoffman degradation process compared to M-nanocomposites due to well restriction of CTAB by clay and rubber. However, releasing of CTAB in the confinement may occur, at the vulcanization step and there by aggregated clay structures may form after de-intercalation of CTAB from inter gallery space of clay [21]. Further, CRI increases with an increase in OMMT loading due to presence of higher degraded CTAB to form more Zn ammine complexes and is greater for M-series compounds. It may be due to effect of both lower crosslink density and higher degraded CTAB. t_{s2} increased due to confinement and t_{90} decreased due to lower crosslink density, finally may give smaller values of t_{90}- t_{s2} and as a result of that CRI of M-series nanocomposite compounds show the highest values.

3.2. Morphology.

Figure 2, Figure 3, Figure 4, Figure 5, Figure 6, Figure 7, Figure 8 and Figure 9 illustrate SEM image of A-0, C-0, A-2, A-5, M-2, M-5, C-2 and C-5 nanocomposites respectively. In the image of A-0, the white colour particles believed to be ordered structures of CTAB and SDS produced by the presence of excess amount of CTAB and SDS, are distributed throughout the rubber matrix. It is believed that ZnO may be also found as whitish particles. However, it is clearly observed that number of whitish particles present in A-0 is greater than those in the image of C-0. In the gelling process, SDS adsorbs on NR latex particles by electrostatic interactions and pre-adsorbed SDS increases polar head to head adsorption between CTAB and SDS. When CTAB is further increased, it would form second layer of CTAB on adsorbed CTAB on latex particle as bi-layer through tail to tail by hydrophobic interactions and thereby ordered structures are formed as suggested by literature [22].

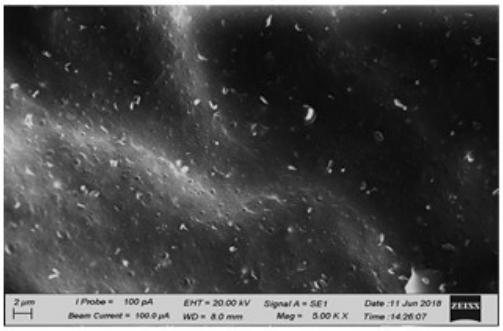

Figure 2. SEM image of A-0

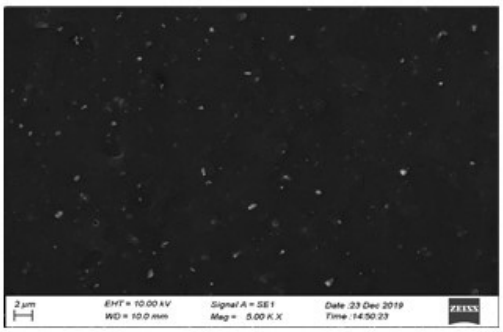

Figure 3. SEM image of C-0

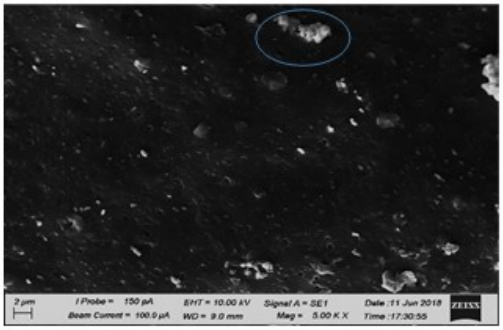

Figure 4. SEM image of A-2 nanocomposite.

SEM images convinced that OMMT dispersed by emulsion blending in A-2 and A-5 nanocomposites are better than mechanical blending in M-2 and M-5 nanocomposites. M-2 and M-5 nanocomposite show aggregated structures and even phase separation of clay from NR. Circles in SEM image show the aggregated structures in nanocomposite. It convinces that incorporation of OMMT into rubber by conventional mixing method is not successful.

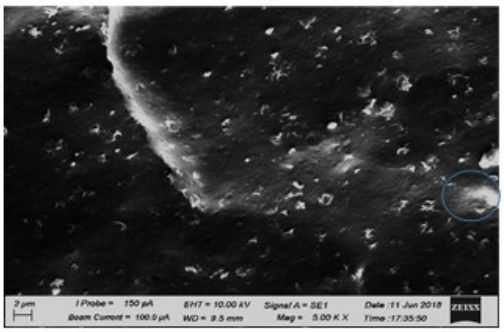

Figure 5. SEM image of A-5 nanocomposite

In A-series nanocomposites, the aggregation structures are minimum and clay structures may be visible as combination of clay and ordered structures. Those structures are not visible in C-series nanocomposites due to absence of gelling agent but it is

seen that less aggregated clay layers dispersed throughout the C-series nanocomposites.

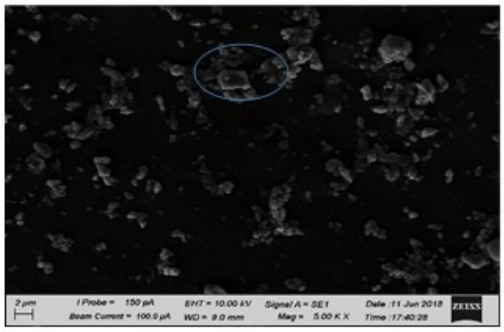

Figure 6. SEM image of M-2 nanocomposite

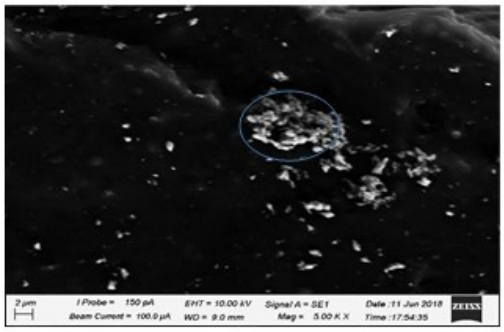

Figure 7. SEM image of M-5 nanocomposite.

3.3. XRD analysis.

Figure 10 displays the XRD diffractograms of nanocomposites-A, nanocomposites-C, nanocomposites-M and respective Controls. Diffractograms of A-0, A-2 and A-5 nanocomposites show peaks at diffraction angles of 4.4 and 6.6.

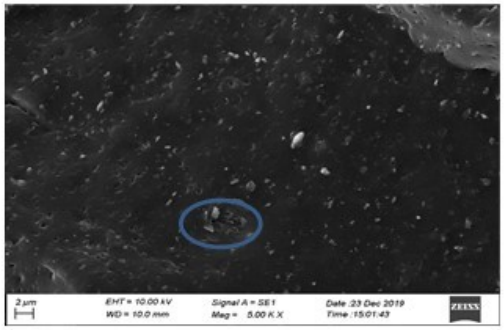

Figure 8. SEM image of C-2 nanocomposite

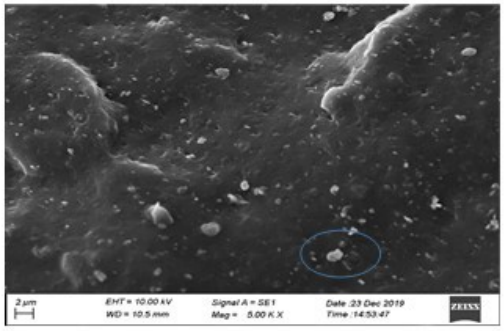

Figure 9. SEM image of C-5 nanocomposite

Those peaks arise due to the presence of crystalline structures formed by the effect of gelling agent which consist of crystalline arrangements of gelling agents and clay. The peaks for corresponding clay structures are not appeared in A-2 nanocomposite due to dominant of crystalline structure of gelling agent.

At a higher OMMT loading, A-5 nanocomposite shows the overlap of peaks corresponding to combination of clay and gelling agents. The evidence, thus suggests that OMMT at higher loading in A-5 nanocomposite may disturb the ordered structures of gelling agent by combination with higher clay layers. The pattern of peak position of M-nanocomposites and C-nanocomposites are almost similar. However, the highest intensity of peaks shown by M-nanocomposites due to the presence of higher aggregation of clay layers.

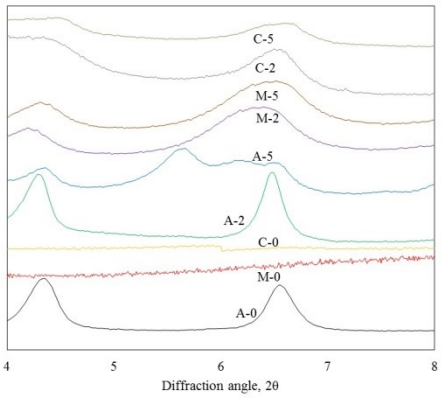

Figure 10. XRD diffractogram of nanocomposites A, C and M.

3.4. Crosslink density.

Figure 11 presents the crosslink density of A, C and M nanocomposites, and their respective Controls.

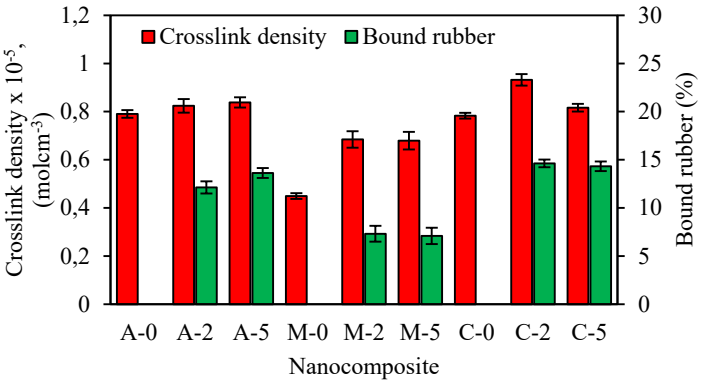

Figure 11. Crosslink density and bound rubber content of different nanocomposites.

The crosslink density of A-nanocomposite and its Control is greater than that of M-nanocomposite and its Control due to the presence of CTAB as a gelling agent in A-nanocomposites and its Control contribution to the formation of a higher amount of zinc-ammine complexes. The higher number zinc-ammine complexes cause an increase of sulphur crosslinks. However, crosslink densities of A-2 and A-5 nanocomposites do not show a significant increase compared to A-0. It may be to reason that dissolution amount of sol in A-2 and A-5 nanocomposites are similar with A-0 due presence of gelling agent. The crosslink density of M-5 nanocomposite should be improved than that of M-2 nanocomposite due to an increase of zinc ammine complexes, but aggregation of OMMT at the higher loading may decrease the crosslink density as suggested by many research [23, 24].

This shows that direct use of mechanical mixing is not a suitable method to incorporate OMMT into rubber even though it is widely used in many industrial applications. The limited amount of CTAB used in C-nanocomposites as intercalation agent in OMMT prevents dissolution as sols and increases the crosslinking density even better than A-nanocomposite.

3.5. Bound rubber.

Bound rubber content of A-2 and A-5 masterbatches is greater than that of M-2 and M-5 masterbatches (Figure 11). The improved compatibility between rubber and OMMT is increased

in A-2 and A-5 masterbatches by use of a higher amount of CTAB under acid-free environment. CTAB forms electrostatic interactions with negatively charged rubber and OMMT. Further, the long chain hydrocarbon tail of CTAB increases organophilisity of hydrophilic clay, thereby it increases rubber-clay interactions. The SDS also would balance those electrostatic interactions and increase the dispersion of OMMT. However, by neglecting the presence of higher content of CTAB and SDS as plasticizers, A-5 masterbatches show higher bound rubber content due to the dominant of improved rubber-clay interactions than plasticizing effect. Instead, a significant reduction of bound rubber content is found in M-masterbatches due to poor interaction between rubber and aggregated OMMT structures under limited CTAB content. However bound rubber content of C-2 and C-5 nanocomposites show the highest values due to less dissolution of sol with the effect of less amount of surfactants present in gelling agent free non-acidic environment.

3.6. DMTA study.

Figure 12 shows tan δ of A-2, C-2 and M-2 nanocomposites.

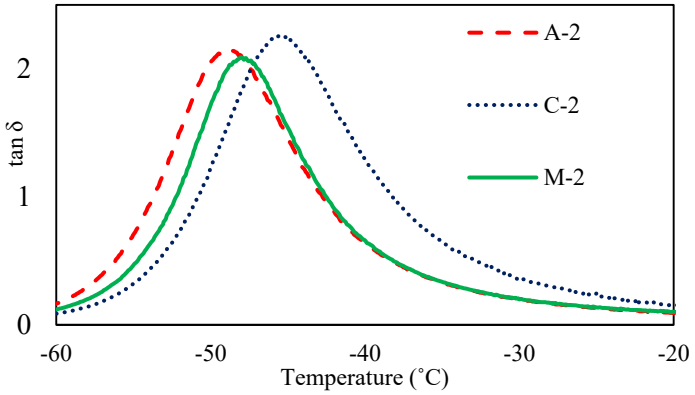

Figure 12. tan δ of A, C and M nanocomposites at 2 phr OMMT loading.

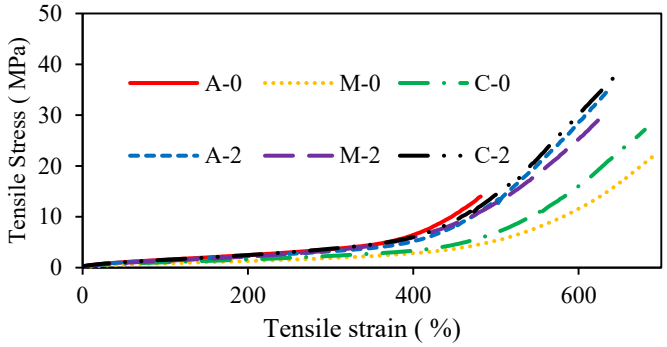

Figure 13. Stress strain curves of A, C and M nanocomposites

This evidence suggests that the presence of OMMT with gelling agent in A-2 nanocomposite lower the T_g (-48.8 ˚C) due to the plasticizing effect of gelling agents. C-2 nanocomposite shows that the highest T_g (-45.4 ˚C) associated with proper OMMT dispersion and caused restriction for mobility of rubber chains. Due to this plasticizing effect of A-nanocomposite caused by gelling agent, T_g decreases. T_g of M-2 nanocomposite (-47.6 ˚C) also decreases due to formation of aggregated clay structures. However, T_g of M-2 nanocomposite is greater than that of A-2 nanocomposite in gelling free environment.

3.7. Mechanical properties.

Stress-strain curves of A-2, C-2 and M-2 nanocomposites and their Controls are shown in Figure 13.

A-0 shows greater strain-induced crystallization than M-0 and C-0, however A-0 breaks early at lower elongation before maximum strain-induced crystallization was achieved. The greater strain-induced crystallization shown by A-0 may be due to the presence of crystalline structures but those were broken at weak interphase between SDS and CTAB in ordered structures while stretching. Therefore, tensile strength and elongation at break of A-0 are reduced by 35% and 55% respectively compared to those of M-0 and are reduced by 50% and 35% respectively compared to those of C-0. C-0 shows higher strain induced crystallization than M-0 mainly due to remaining of higher non-rubber content by AFCC method.

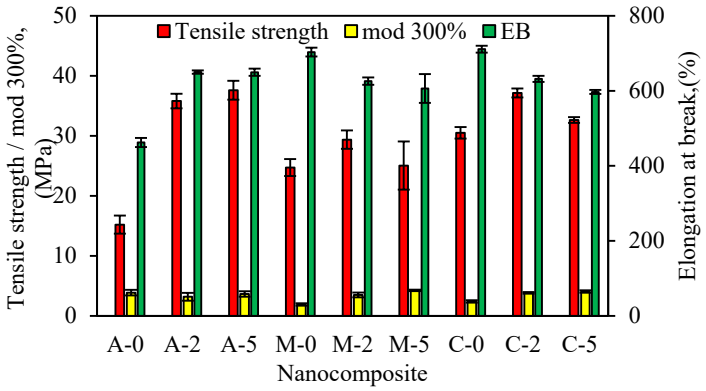

Figure 14. Tensile properties of A, C and M nanocomposites.

Many works in literature described that strain-induced crystallization is increased at higher non-rubber substances [25,26]. It is believed that non-rubber substances were removed during preparation of pale crepe while removal of water in processing stage. However, non-rubber content in NRL remains in A-series and C-series nanocomposites because water was only removed by evaporation at the drying stage. Strain-induced crystallization of both C-2 and M-2 nanocomposite show a similar trend but M-2 nanocomposite breaks early at comparative lower elongation to A-2 nanocomposite.

Figure 14 presents the tensile strength, elongation at break, and mod 300% of A, C and M nanocomposites.

The lower tensile strength and elongation at break in A-0 cause due to fracture initiation at weak interphase between CTAB and SDS in ordered structures. However, with the addition of OMMT, A-nanocomposites increase its tensile strength and elongation at break due to reinforcement effect, which is different from M-nanocomposites and C-nanocomposites. It is interesting to point out that fracture initiation points in interphase of gelling structures reduced by reinforcement of OMMT, which would give greater improvement of such properties in A-nanocomposite compared to that of its Control. Further, the tensile strength of A-2 and A-5 nanocomposites are increased by 22% and 26% compared to that of M-2 and M-5 nanocomposites respectively. With the further addition of OMMT, at 5 phr, the tensile strength of A-5 nanocomposite is further increased but tensile strength of M-5 nanocomposite is reduced. It shows that presence of higher amount of aggregated structures in M-5 nanocomposite decreases the tensile strength and elongation at break than that of M-2 nanocomposite. However, tensile strength of M-5 nanocomposite is comparatively high due to better dispersion of OMMT with minimum aggregation, thereby reinforcement is further increased.

This evident shows that preparation of masterbatches by AFCC method in A-nanocomposites is more effective than for masterbatches prepared by mechanical mixing. Elongation at break of C-0 and M-0 are the highest due to less disturbance of structure of rubber. Elongation at break of nanocomposites are not deviated differently with each other even though tensile strength shows different values. This shows that better dispersion of nanoclay may increase the tensile strength. The improved slippery action of OMMT with the effect of gelling agent in A-2 and A-5 nanocomposite may also increase the elongation at break [27]. However, A-5 shows the highest tensile strength (37.6 MPa), with the effect of better dispersion of higher number of clay layers with minimum aggregation.

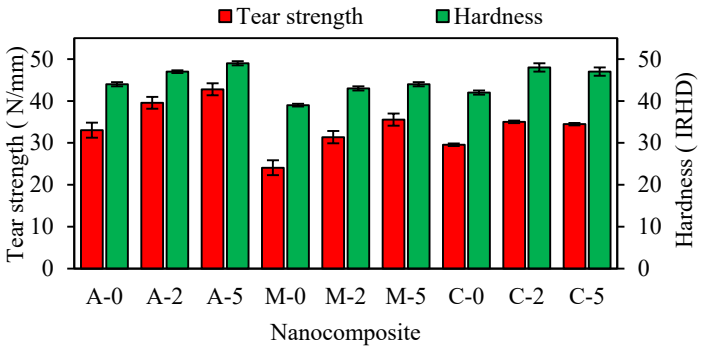

Figure 15. Tear strength and Hardness of different nanocomposites.

The mod 300% of A-0 is 103% greater than that of M-0 due to higher crosslink density in A-0. Interestingly, with the addition of OMMT, the mod 300% of A-2 and A-5 nanocomposites decrease than that of M-2 and M-5 nanocomposites, which may be due to an increased plasticization effect by gelling agent in A-nanocomposites. It is further convinced that the gelling agent free environment in C-nanocomposites, mod 300% of C-2 and C-5 are greater than 20% and 11% respectively with compared to A-2 and A-5 nanocomposites. Further, it is noticed that the mod 300% of each nanocomposite at 5 phr is greater than that of 2 phr due to reinforcement of filler effect.

Figure 15 illustrates the tear strength and hardness of A-nanocomposites, C-nanocomposites, M-nanocomposites and their Controls.

It is interesting to note that A-nanocomposites and control show comparatively higher tear strength than other two nanocomposites and Control even though presence of gelling agent presence in A-nanocomposite. Propagation of tear path does not break at weaker interphases in ordered structures, whereby it travels between such interphases for longer distance to obtain moderately higher tear strength. Both nanocomposites show higher tear strength than respective Controls by mean of better dispersion of clay. It is further confirmed that tear strength of A-5 nanocomposite shows higher tear strength (42.7 N/mm), which is 20% greater than that of M-5 nanocomposite, and the A-2 nanocomposite is 26% greater than that of M-2 nanocomposite.

The hardness of A-0 is 12.8% greater than that of M-0 and is mainly due to an increase of crosslink density. Hardness is further increased by the addition of OMMT in each nanocomposites than their corresponding Controls by filler effect. A-5 nanocomposite shows the highest hardness (49 IRHD), which is 11.3% higher than that of M-5 nanocomposites and 5% higher than C-5 nanocomposite. These results imply that hardness is not reduced by the plasticizing effect with the addition of gelling agent, but is due to an increase of crosslink density and bound rubber content.

4. CONCLUSIONS

The slow drying problem in AFCC method was successfully solved by introduction of gelling agents in A series nanocomposites. Gelling agents used in A series reduced the T_{s2} and T_{90} in the cure properties. SEM and XRD confirmed that ordered structures were formed in control sample of A-series. The ordered gelling structures are disturbed by better dispersion of OMMT at 5 phr loading, thereby clay gelling structures were formed. A better dispersion of higher number of clay layers increased tensile strength with less reduction of elongation at break, tear strength and hardness under acid free gelling environment. The use of gelling agent increased the rate of drying in AFCC method and improved better dispersion of clay layers. The weak interface of between CTAB and SDS in ordered structures was strengthened by reinforcement of clay. Bound rubber, crosslink density and T_g were reduced when gelling agent was added but it did not cause undesirable effect for reducing mechanical properties of nanocomposite. However, mechanical properties, crosslink density, bound rubber of nanocomposite prepared by only mechanical mixing were inferior to nanocomposite prepared by AFCC method using the combined gelling agent.

5. REFERENCES

1. Le, M.T.E.F. Influence of nanosilica in mechanical property of natural rubber composite, 4th international conference on green technology and sustainable development, Ho Chi Minh City, Vietnam, 23-24 Nov 2018, IEEE, http://doi.org/10.1109/GTSD.2018.8595529.
2. Otaikhian K.S.; Adeniyi, A.G.; Dada A.M.; Ighalo, J. Assessment of carbonized wood-flour fillers on mechanical properties of natural rubber vulcanizates. *Eur,j.sustain.dev*. **2019**, *3*, em0097, http://doi.org/10.29333/ejosdr/5860.
3. Meera, A.P.; Thomas, S.; Zachariah, A.K.; Yang, W. Effect of organoclay on the solvent diffusion behavior and mechanical properties of natural rubber nanocomposites. *Polym.Compos*. **2018**, *39*, 3110-3118, https://doi.org/10.1002/pc.24317.
4. Ravikumar, K.; Joseph, R.; Ravichandran, K. Effect of organo clay on curing, mechanical and dielectrical properties of NR/SBR blends. *National conference on mathematical techniques and its application, J.Phys.conf.ser* **2018**, *1000,* http://doi.org/10.1088/1742-6596/1000/1/012116.
5. Chouytan, J.; Kalkornsurapranee. E.; Fellows, C.M.; Kaewsakul, W. In situ modification of polyisoprene by organo-nanoclay during emulsion polymerization for reinforcing natural rubber thin films. *Polymers* **2019**, *11,* 1338-1359, https://dx.doi.org/10.3390%2Fpolym11081338.
6. Fathurrohman, M.I.; Rugmai, R.; Hayeemasae, N.; Sahakaro, K. Dispersion and properties of natural rubber-montmorillonite nanocomposite fabricated novel in situ orgonomodified and latex

compounding method. *Polym. eng. sci.* **2019**, *59,* 1830-1839, http://doi.org/10.1002/pen.25183.
7. Pajarito, B.B. Differentiation of non-black fillers in rubber composites using linear discriminant analysis of principal components. *Sci.eng.compos.mater*. **2019**, *26*, 282-291, http://doi.org/10.1515/secm-2019-0010.
8. Zachaiah A.K.; Chandra A.K.; Mohammed, P.K.; Thomas, S. Vulcanization kinetics and mechanical properties of organically modified nanoclay incorporated natural and chlorobutyl rubber nanocomposites. *Polym. Test*. **2019**, *76*, 154-165, http://doi.org/10.1016/j.polymertesting.2019.02.003.
9. Pinnavaia, T.G.; Beall, G.W.; B. *Polymer-clay nanocomposite.* 1st ed.; Willy: New York, USA, 2001; pp. 3-9.
10. Lopez-Manchado, M.A.; Arroyo, M.; Herrero, B.; Biagiotti, J. Vulcanization kintics of natural rubber organoclay nanocomposites. *J.Appl.Polym.Sci.* **2003**, *89*, 1-15, http://doi.org/10.1002/app.12082.
11. Vaia, R.A.; Ishil, H.; Giannelis, E.P. Synthesis and properties of two dimentional nanostrutures by direct interaction of polymer melts in layered silicates. *Chem.Mater.* **1993**, *5*, 1694-1696, http://doi.org/10.1021/cm00036a004.
12. Rezende, C.A.; Braganca, F.C.; Doi, T.R.; Lee, L.; Galebeck, F.; Baue, F. Natural rubber clay nanocomposites: mechanical and structural properties. *Polym J.* **2010**, *51*, 3644-3652, http://doi.org/10.1016/j.polymer.2010.06.026.
13. Jayaraj, S.; Egodage, S.M; Walpalage, S. Incoporation of nanoclay into field latex to develop nanoclay filled dry rubber compound. *Natl. Sci. Found. Sri.* **2017**, 121-132, http://doi.org/10.4038/jnsfsr.v45i2.8178.
14. Jayaraj, S.; Egodage, S.M.; Walpalage, S. New approach for preparation of dry natural rubber nanocomposites through acid-free co-coagulation: Effect of organoclay content, *J.Appl.Polym.Sci.* **2018**, *135*, http://doi.org/10.1002/app.46502.
15. Cova, M.; Fernandez, A.; Carcia, D.; Bacigalupe, A.; Sanchez, R.M.T.; Escobar, M. Acrylonitrile butadiene nanocomposites containing different clays by latex compounding method. *Polym.Eng.Sci*. **2018**, *59,* 736-744, http://doi.org/10.1002/pen.24991.
16. Merad, B.; Bekkour, K.; Gareche, M. Rheological and structural characterization of organo-hectorite dispersions:influence of the organoclay loading. *Appl.Clay.Sci*, **2020**, *184,* in press, http://doi.org/10.1016/j.clay.2019.105321.
17. Flory P.J.; Rehner, J.R.; Statistical mechanics of cross-linked polymer networks II. Swelling. *J. Chem. Phys.***1943**, *11*, 521-526, http://doi.org/10.1063/1.1723792.
18. Ellis, B.; Welding, G.N. Estimation from swelling of the structural contribution of chemical reactions to the vulcanization of natural rubber II. Estimation of equlibrium degree of swelling, *Rubber. Chem. Technol.* **1964**, *37*, 571-575, http://doi.org/10.5254/1.3540349.
19. Lopez-Manchado, M.; Herrero, B.; Arroyo, M. Organoclay-natural rubber nanocomposites synthesized by mechanical and solution mixing method. *Polym. Int.* **2004**, *53*, 1766-1772, http://doi.org/10.1002/pi.1573.
20. Xie, W.; Gao, Z.; Pan, W.; Hunter, D.; Singh, A.; Vaia, R. Thermal degradation chemistry of alkyl quaternary ammonium montmorillonite, *Chem. Mater.* **2001**, *13*, 2979-2990, http://doi.org/10.1021/cm010305S.
21. Varghese, S.; Karger-kocsis, J. Natural rubber-based nanocomposites by latex compounding with layered nanocomposites by latex compounding with layered silicates, *Polymer*, **2003**, *44*, 4921-4927, http://doi.org/10.1016/S0032-3861(03)00480-4.
22. Pongnara, P.; Poonsawat, C.; Amnuaypanich, S. Adsorption study of surfactant on natural rubber latex particles. *APSI.* **2008**, *13*, 694-700.
23. Arroyo, M.; Lopez-manchado, M.A.; Herrero, B. Organo-montmorillonite as subtitute of carbon black in natural rubber compounds. *Polymer*. **2003**, *44*, 2247-2453, https://doi.org/10.1016/S0032-3861(03)00090-9.
24. Vijayalekshmi, V.; George, K.E.; Pavithra, C. Studies on maleated natural rubber/ organoclay nanocomposites. *Prog. Rubber. Plast. Re*. **2010**, *26*, 183-198, http://doi.org/10.1177/147776061002600403.
25. Amnuaypornsri, S.; Sakadapipanich, J.; Toki, S.; Hsiao, B.S.; Ichikawa, N.; Tanaka, Y. Strain-induced crystallization of natural rubber: effect of proteins and phospholipids. *Rubber. Chem. Technol*. **2008**, *81*, 753-766. https://doi.org/10.5254/1.3548230.
26. Tosaka, M.; Farutani, M.; Tsuji, M.; Ikeda, Y.; Kohjiya, S.; Wititsuwannakul, G.; Wititsuwannakul., D.; Nagayama, K.; Danev, R. Strain induced crystallization of fractionated natural rubber from fresh latex. *J. Soc. Mater. Sci*. **2009**, *58*, 5-10, https://doi.org/10.2472/jsms.58.5.
27. Wu, Y.; MA, Y.; Wang, Y.; Zhang, L.; Effect of characteristics of rubber, mixing and vulcanization on the structure and properties of rubber/ clay nanocomposites by melt melting. *Macromol. Mater. Eng*. **2004**, *289*, 890-894, http://doi.org/10.1002/mame.200400085.

6. ACKNOWLEDGEMENTS

This research project was supported by the Senate Research Committee of the University of Moratuwa under the grant number SRC/CAP/14/05. We would like to thank technical officer Mr. M.T.M.R Jayaweera for his support on experimental work.